Hyperglycemia-Induced Changes in ZIP7 and ZnT7 Expression Cause Zn^{2+} Release From the Sarco(endo)plasmic Reticulum and Mediate ER Stress in the Heart

Erkan Tuncay,[1] Verda C. Bitirim,[1] Aysegul Durak,[1] Gaelle R.J. Carrat,[2] Kathryn M. Taylor,[3] Guy A. Rutter,[2] and Belma Turan[1]

Diabetes 2017;66:1346–1358 | DOI: 10.2337/db16-1099

PATHOPHYSIOLOGY

Changes in cellular free Zn^{2+} concentration, including those in the sarco(endo)plasmic reticulum [S(E)R], are primarily coordinated by Zn^{2+} transporters (ZnTs) whose identity and role in the heart are not well established. We hypothesized that ZIP7 and ZnT7 transport Zn^{2+} in opposing directions across the S(E)R membrane in cardiomyocytes and that changes in their activity play an important role in the development of ER stress during hyperglycemia. The subcellular S(E)R localization of ZIP7 and ZnT7 was determined in cardiomyocytes and in isolated S(E)R preparations. Markedly increased mRNA and protein levels of ZIP7 were observed in ventricular cardiomyocytes from diabetic rats or high-glucose–treated H9c2 cells while ZnT7 expression was low. In addition, we observed increased ZIP7 phosphorylation in response to high glucose in vivo and in vitro. By using recombinant-targeted Förster resonance energy transfer sensors, we show that hyperglycemia induces a marked redistribution of cellular free Zn^{2+}, increasing cytosolic free Zn^{2+} and lowering free Zn^{2+} in the S(E)R. These changes involve alterations in ZIP7 phosphorylation and were suppressed by small interfering RNA–mediated silencing of CK2α. Opposing changes in the expression of ZIP7 and ZnT7 were also observed in hyperglycemia. We conclude that subcellular free Zn^{2+} redistribution in the hyperglycemic heart, resulting from altered ZIP7 and ZnT7 activity, contributes to cardiac dysfunction in diabetes.

Diabetes is an important risk factor for cardiovascular dysfunction through defective Ca^{2+} signaling (1,2). However, we have previously shown that Zn^{2+} release during the cardiac cycle results in cytosolic free Zn^{2+} increase (3), further triggering higher prooxidant species production that leads to oxidative damage (4). Conversely, oxidant exposure induces marked cytosolic free Zn^{2+} increases in cardiomyocytes (5), whereas hyperglycemia causes oxidative stress and increased cytosolic Zn^{2+} through underlying cardiac dysfunction (6). Similar to Ca^{2+}, Zn^{2+} is essential for cellular functions in mammalian heart (7), serving as an important secondary messenger (8).

Excess Zn^{2+} can be detrimental to cells, particularly that of cardiomyocytes (3,5–7). Cytosolic Zn^{2+} plays an important role in excitation-contraction coupling in cardiomyocytes by shaping Ca^{2+} dynamics (3,4,9). Its level in cardiomyocytes is calculated as <1 nmol/L, but it is approximately fivefold higher in sarco(endo)plasmic reticulum [S(E)R] and less than the cytosolic level in mitochondria, as demonstrated previously with Förster resonance energy transfer (FRET) recombinant-targeted Zn^{2+} probes (10). Elevated cytosolic Zn^{2+} appears to contribute to deleterious changes in many cellular signaling pathways, including hyperglycemia-challenged cardiomyocytes (3–6,11).

Cellular Zn^{2+} fluxes are achieved and controlled by Zn^{2+} transporters (ZnTs) and Zn^{2+} importers (ZIPs) (12,13), although their distributions and functions are not yet well clarified in cardiomyocytes. The Zn^{2+}-selective ion channel ZIP7 plays an important role in releasing Zn^{2+} from the S(E)R and Zn^{2+}-associated induction of unfolded protein

[1]Department of Biophysics, Faculty of Medicine, Ankara University, Ankara, Turkey
[2]Section of Cell Biology and Functional Genomics, Division of Diabetes, Endocrinology and Metabolism, Department of Medicine, Imperial College London, London, U.K.
[3]School of Pharmacy and Pharmaceutical Sciences, College of Biomedical and Life Sciences, Cardiff University, Cardiff, U.K.

Corresponding author: Belma Turan, belma.turan@medicine.ankara.edu.tr, or Guy A. Rutter, g.rutter@imperial.ac.uk.

Received 10 September 2016 and accepted 10 February 2017.

This article contains Supplementary Data online at http://diabetes.diabetesjournals.org/lookup/suppl/doi:10.2337/db16-1099/-/DC1.

G.A.R. and B.T. are equal senior authors.

© 2017 by the American Diabetes Association. Readers may use this article as long as the work is properly cited, the use is educational and not for profit, and the work is not altered. More information is available at http://www.diabetesjournals.org/content/license.

response in yeast (14) and is localized to the Golgi apparatus in CHO cells, allowing Zn^{2+} release from Golgi lumen into cytosol (15). ZIP7 facilitates the release of Zn^{2+} from the ER (16) and behaves as a critical component in subcellular redistribution of Zn^{2+} in other systems (17). In addition, protein kinase 2 (CK2) has been hypothesized to trigger cytosolic Zn^{2+} signaling pathways by phosphorylating ZIP7 (18), although some studies have also highlighted its important contribution to Zn^{2+} homeostasis under pathological conditions (19–21).

Although studies have shown the presence of weakly expressed ZIP7 and ZnT7 in mammalian heart (22,23), their subcellular localizations and functional roles are not yet known well. In that regard, previous studies have suggested that either an increase or an inhibition of one of them might contribute to cellular dysfunction (11), including defective insulin-mediated signaling pathways under hyperglycemia (24) or altered insulin secretion (25,26).

ER stress is one of underlying mechanisms of cardiac dysfunction, including diabetic cardiomyopathy (27–29). Studies suggest that a relationship exists between S(E)R function and cytosolic Zn^{2+} level in diabetic (DM) rat cardiomyocytes (29,30). In particular, the latter studies identified a close association among oxidative stress, cytosolic Zn^{2+} increase, ER stress, and cardiac dysfunction in diabetes. However, experimental evidence suggests a requirement for Zn^{2+} for proper ER function, with Zn^{2+} deficiency leading to ER stress (14,31) from decreased Zn^{2+} in the ER as a result of hypoxia or hypoglycemia (14). However, no clear data demonstrate which ZnTs play roles in controlling cytosolic Zn^{2+} increases in cardiomyocytes during hyperglycemia.

Thus, hypothesizing that disruption of ZnTs and the Zn^{2+} axis contributes to deleterious changes in diabetic cardiomyocytes is tempting. We aimed to first clarify their subcellular localizations and then to explore their functional roles in Zn^{2+} homeostasis. In addition, we tested their roles in cytosolic Zn^{2+} redistribution and development of ER stress under hyperglycemic conditions as a result of CK2α activation.

RESEARCH DESIGN AND METHODS

Diabetes Induction

This study was approved by the Ankara University (Ankara, Turkey) ethics committee (115-449). Type 1 diabetes was mimicked by single injection of streptozotocin (50 mg/kg i.p.; Sigma-Aldrich) in 3-month-old male Wistar rats (n = 15), whereas control rats (n = 10) were injected with vehicle as previously described (2). After streptozotocin injection (7 days), rats with threefold higher blood glucose levels compared with preinjection levels were used as the DM group (n = 13 kept for 12 weeks).

Cardiomyocyte Isolation

Cardiomyocytes were isolated from the left ventricle by using the enzymatic method as previously described (5). Hearts were cannulated on a Langendorff apparatus, leaving preperfusion through the coronary artery with a Ca^{2+}-free solution. Preperfusion was followed with 1 mg/mL of collagenase (Type 2; Worthington Biochemical Corporation, Lakewood, NJ)-containing solution for 30–35 min. Only Ca^{2+}-tolerant rod-shaped cells were used to ensure cell viability and excitability as well to avoid SR Ca^{2+} overload and terminal contracture.

Cell Culture

The embryonic rat heart–derived H9c2 cell line was purchased from ATCC (Manassas, VA) and was cultured in DMEM as previously described (10).

Cytosolic and S(E)R Free Zn^{2+} Levels

Cytosolic and S(E)R free Zn^{2+} levels ($[Zn^{2+}]_{Cyt}$ and $[Zn^{2+}]_{ER}$, respectively) in H9c2 cells were measured with eCALWY sensors (Cyt-eCALWY4 and ER-eCALWY6, respectively) delivered with plasmids expressing Cyt-eCALWY4 and ER-eCALWY6. Measurements were performed as previously described (10). Images were captured at the 433-nm monochromatic excitation wavelength, and image analysis was performed with ImageJ software by using a custom-made macro. To calculate free Zn^{2+}, maximum (R_{max} by using a heavy metal chelator, TPEN [N,N,N′,N′-tetrakis(2-pyridylmethyl) ethylenediamine] 50 μmol/L; Sigma-Aldrich) and minimum (R_{min} by using Zn^{2+} saturation with 100 μmol/L $ZnCl_2$ and Zn^{2+} ionophore pyrithione (Zn^{2+}/Pyr 5 μmol/L) fluorescence ratios were used as previously described (13).

Imaging Subcellular Localization of ZIP7 and ZnT7

ZIP7 and ZnT7 localizations were determined by using anti-ZIP7 and anti-ZnT7 antibodies (PA5-21072 [Thermo Fisher Scientific] and sc-160946 [Santa Cruz] at 1:50, respectively) in confocal microscopy (LSM510; Zeiss). S(E)R localization was determined by transfection of H9c2 cells with ER-resident *Discosoma* species red fluorescent protein (DsRed-ER) (red) plasmid for 24 h. After performing general procedures, cells were incubated with specific antibodies to monitor their localizations. After overnight incubation, cells were incubated with appropriate secondary antibodies in the presence of BSA (5%; Alexa Fluor 488 donkey anti-rabbit and donkey anti-goat 1:1,000 for ZIP7 and ZnT7, respectively).

The Golgi apparatus was labeled with an anti-GM130 antibody *cis*-Golgi marker (ab52649 1:750; Abcam). Cells were then incubated either with anti-ZIP7 or with anti-ZnT7 and Golgi marker GM130 antibody for ZIP7 and ZnT7 (secondary antibodies: Alexa Fluor 488 donkey anti-rabbit 1:1,000 for ZIP7, Alexa Fluor 568 goat anti-mouse 1:1,000 for GM130, Alexa Fluor 488 donkey anti-goat 1:1,000 for ZnT7, and Alexa Fluor 647 rabbit anti-mouse 1:1,000 for GM130). Finally, cells were mounted with medium containing DAPI (blue). Images were deconvolved and analyzed for their colocalizations with use of Huygens software (https://svi.nl/HuygensProfessional) and processed with ImageJ software.

S(E)R Isolation

Left-ventricular S(E)R fractionation of hearts was performed by using an ER Isolation Kit (E0100; Sigma). Briefly, hearts were homogenized in isotonic extraction buffer and then centrifuged. Crude microsomal fraction was isolated from postmitochondrial fraction by using ultracentrifugation. For further purification and separation for rough ER and

smooth ER, a self-generating density gradient procedure was performed according to the manufacturer's instructions. Western blot analysis was carried out by using primary antibodies against ZIP7 and ZnT7. To confirm S(E)R-isolation, SERCA2 (sc-8094; Santa Cruz), Golgi 58K Protein (ab27043; Abcam), and cyclin E (sc-481; Santa Cruz) were used as S(E)R, Golgi, or nuclear markers, respectively.

ZIP7 Silencing in H9c2 Cells With Stable Lentiviral Infection

H9c2 cells were stably transfected with four unique 29-mer short hairpin RNA (shRNA) constructs in lentiviral RFP (red fluorescent protein) vector (SR02938179A, B, C, and D; Origene) and noneffective 29-mer scrambled shRNA (sc-shRNA) cassette in pRFP-CB-shLenti vector as control (TR30033; Origene). Twenty-four hours before transfection, cells were seeded into separate dishes. Every shRNA construct with packaging and enveloping plasmids (psPAX [Addgene 12260] and pMD2G [Addgene 12259]) were mixed into a solution containing $CaCl_2$ (375 mmol/L) and then incubated for 30 min. DNA mixtures were added into HEPES buffer saline containing (in mmol/L) 12 dextrose, 50 HEPES, 10 KCl, 280 NaCl, and 1.5 $Na_2HPO_4H_2O$; every mixture was added into separate 15-cm dishes and incubated for 12 h. Viral supernatants were harvested after 24 h and 48 h, and cells were then infected with each lentivirus produced from every shRNA construct, including scrambled sequences at 3 plaque-forming units/cell (incubation with 10 μg/mL blasticidin for antibiotic selection). They were seeded into six-well plates and harvested for knockdown efficiency to measure ZIP7 mRNA levels (Supplementary Table 1). A mixture of four ZIP7 gene-specific shRNA constructs was used.

Quantitative RT-PCR Analysis

Total RNA was prepared by using an RNA Isolation Kit (740955.10; Macherey-Nagel), and purified total RNA was reverse transcribed with a ProtoScript First Strand cDNA Synthesis Kit (E6300S; New England Biolabs). First-strand cDNAs were quantified with GoTaq qPCR Master Mix (A6001; Promega). The amplified fragment size of PCR products for each primer and for all primers' specificity were controlled for through the National Center for Biotechnology Information and Ensembl databases. Primer sequences for cyclophilin, ZIP7, and ZnT7 are listed in Supplementary Table 2. The fold changes in the genes were analyzed by comparative ($2^{-\Delta\Delta Ct}$) method.

Western Blot Analysis

The lysates were extracted with NP-40 lysis buffer (250 mmol/L NaCl, 1% NP-40, and 50 mmol/L Tris-HCl; pH 8.0 and 1 × protease inhibitor cocktail) from homogenized samples. Protein concentration of supernatants (centrifuged at 12,000*g* for 5 min at 4°C) was measured with a BCA Assay Kit (Pierce). Equal amounts of protein were separated on 12% SDS-PAGE Tris-Glycine or 4–12% NuPAGE Bis-Tris Protein Gels (Life Technologies). The membranes were probed with antibodies against GRP78 (sc-13968 1:200; Santa Cruz), Calregulin (CALR) (sc-11398 1:200; Santa Cruz), ZIP7 (sc-83858 1:200; Santa Cruz), ZnT7 (sc-160946 1:200; Santa Cruz), SERCA2 (sc-8094 1:200; Santa Cruz), Golgi 58K Protein (ab27043 1 μg/mL; Abcam), cyclin E (sc-481; Santa Cruz), GAPDH (sc-365062 1:1,000; Santa Cruz), pZIP7 (a mouse monoclonal antibody to pS275S276-ZIP7, which recognizes ZIP7 only when phosphorylated on residues at S275 and S276, from K.M.T.) and β-actin (sc-47778 1:500; Santa Cruz) in BSA, PBS, and Tween 20 solution. Specific bands were visualized with horseradish peroxidase–conjugated compatible secondary antibodies (anti-mouse 1:2,000, anti-goat 1:7,500, anti-rabbit 1:7,500) and detected by Immuno-Cruz Western Blotting Luminol Reagent (sc-2048; Santa Cruz). The band densities were analyzed with ImageJ software.

Coimmunoprecipitation

Cells were treated as indicated and lysed in coimmunoprecipitation buffer containing (in mmol/L) 50 Tris, 100 NaCl, 1 EDTA, 1% Triton-X 100, and 10% glycerol (pH 7.4); protease inhibitors (1 mmol/L phenylmethylsulfonyl fluoride and 1 μg/mL each of leupeptin, aprotinin, and pepstatin); and phosphatase inhibitors (10 mmol/L sodium-fluoride and 1 mmol/L sodium orthovanadate) for 30 min at 4°C. The 600-μg protein lysates from aliquots (1 mL lysis buffer) were precleared through incubation with 30 μL Protein A/G Sepharose (Sigma) for 1 h at 4°C. The precleared samples were incubated with specific primary antibody (anti-CK2α 10 μg/mL, sc-6480; Santa Cruz) in lysis buffer for 2 h at 4°C and then 30 μL Protein A/G beads were added. Samples were then incubated overnight at 4°C, and beads were washed five times with lysis buffer, boiled, and separated by 10% SDS-PAGE.

CK2α Silencing in H9c2 Cells

CK2α (1 and 2) was silenced in H9c2 cells by using Lipofectamine 2000 (Thermo Fisher Scientific) according to the manufacturer's small interfering RNA (siRNA) transfection protocol. Briefly, cells were seeded into six-well plates and cultured for 48 or 72 h with a mixture of 25 nmol/L CK2α1 and CKα2 or nontargeted siRNAs (ON-TARGETplus SMARTpool Csnk2a1 and Csnk2a2-siRNA and ON-TARGETplus Non-targeting Control Pool, L-096197-02-0005, L-092756-02-0005, and D-001810-10-05, respectively; Dharmacon) with serum-free medium that included 5 μL/mL Lipofectamine. After incubation, the cells were extracted into buffers to examine protein and mRNA expression levels. The primer sequences designed for CK2α1 and CKα2 are listed in Supplementary Table 2.

Statistics

Data are presented as mean ± SEM unless otherwise stated. Differences were determined using Student *t* tests with Bonferroni correction for multiple comparisons as required. GraphPad Prism 6.0 statistical software was used for the analyses. $P < 0.05$ was considered significant.

RESULTS

Regulation of ZIP7 and ZnT7 Expressions by High Glucose

Protein and mRNA levels of ZIP7 (at 50 kDa) and ZnT7 (at 42 kDa) in isolated rat ventricular cardiomyocytes are

shown in Fig. 1*A* and *B*. Both mRNA and protein levels of ZIP7 were significantly increased in DM rat cardiomyocytes, with significantly decreased ZnT7 levels. To test these changes that directly arose through hyperglycemia, we incubated isolated cardiomyocytes under high glucose (33 mmol/L) conditions for 3 h and then compared ZIP7 and ZnT7 with that of mannitol (23 mmol/L)-incubated cells. Similar changes were found in mRNAs to those of DM rat cells, except for their protein levels (~10%) (Supplementary Fig. 1), which was probably due to shorter high-glucose exposure compared with diabetes.

For further validation, we used high-glucose–incubated (25 mmol/L for 24 h) H9c2 cells and measured protein and mRNA levels. As can be seen in Fig. 1*C* and *D*, both levels of ZIP7 increased significantly in high-glucose–incubated cells, whereas the ZnT7 mRNA level (Fig. 1*D*) was markedly (~75%) decreased with a relatively small decrease (~25%) in its protein level.

Next, we performed experiments to determine whether the expression of other ZnTs, such as ZIP1, ZIP6, ZnT1, and ZnT5, were affected in hyperglycemic cardiomyocytes. By using quantitative RT-PCR, we demonstrated that mRNA levels of these transporters were not significantly altered in high-glucose–incubated versus control cells (25 mmol/L for 24 h) (Supplementary Fig. 2*A* and *B*).

High Glucose Induces ZIP7 Phosphorylation

Since the use of a specific antibody developed by one of us (K.M.T.) in breast cancer cells (18), we examined the possible dependency of ZIP7 phosphorylation on hyperglycemia in both DM rat cardiomyocytes and high-glucose–incubated H9c2 cells (25 mmol/L for 24 h or 48 h). As shown in Fig. 1*E*, phospho-ZIP7 (pZIP7) levels measured at about 50 kDa in DM rat cells was about sevenfold higher compared with controls. Furthermore, the pZIP7 level in high-glucose–incubated H9c2 cells was higher compared with nonincubated cells in a time dependent manner (Fig. 1*F*). The pZIP7/ZIP7 ratio was similar in high-glucose–incubated H9c2 cells and higher for DM rat heart (0.96 ± 0.04 vs. 4.79 ± 0.39, respectively).

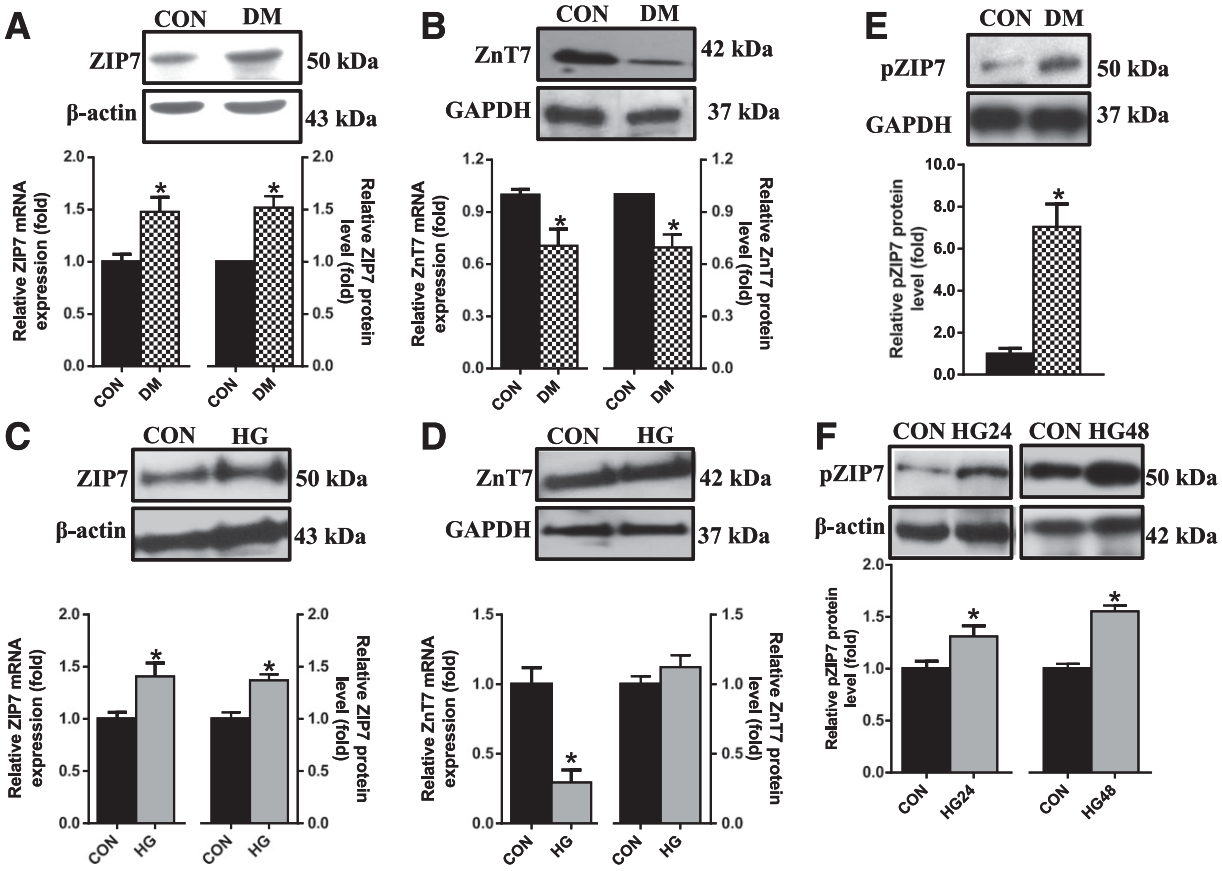


Figure 1—mRNA expression and protein levels of ZIP7 and ZnT7 in cardiomyocytes from either DM rat heart or hyperglycemic H9c2 cells. *A* and *B*: The mRNA and protein levels of ZIP7 and ZnT7 in ventricular cardiomyocytes isolated from either DM or control (CON) rats (RESEARCH DESIGN AND METHODS). *C* and *D*: The mRNA expression and protein levels of ZIP7 and ZnT7 from high-glucose (HG)–incubated (25 vs. 5.5 mmol/L for 24 h) H9c2 cells. Densitometric analysis (above the graphs) shows that ZIP7 and ZnT7 are expressed at ~50 and 42 kDa, respectively. *E* and *F*: The ZIP7 phosphorylation in cardiomyocytes under chronic hyperglycemia (DM group) compared with the CON group and H9c2 cells incubated with HG (25 mmol/L for 24 or 48 h). The phosphorylation levels of ZIP7 are measured by using the pZIP7 antibody developed by K.M.T.'s laboratory and compared with their CON. Data are mean ± SEM. Number of samples (n = 5–6 for hearts per group per protocol) and measurements with double assays in each sample from each group for each type of measurement are shown. *$P < 0.05$ vs. CON.

ZIP7 and ZnT7 Localize to the S(E)R

ZIP7 and ZnT7 have been reported in mammalian heart (22,23) and proposed to localize to the ER (17,21,25) and/or perinuclear vesicles associated with the Golgi apparatus (22,24) in cells but not in cardiomyocytes. Furthermore, ZIP6 and ZIP7 have been shown to colocalize to the ER regulating cytosolic Zn^{2+} homeostasis in dispersed pancreatic islet cells (19). In the current study, we postulated a similar endogenous subcellular localization for ZIP7 and ZnT7 to S(E)R in H9c2 cells. Therefore, after transfection with DsRed-ER (RESEARCH DESIGN AND METHODS), ZIP7 or ZnT7 localizations to S(E)R were visualized. Individual and merged confocal images are shown in Fig. 2*A* and *B*. The merged visual inspections show the presence of the majority of ZIP7 and ZnT7 in the S(E)R. For colocalization, Pearson correlation coefficients were calculated for ZIP7 and ZnT7 associated with S(E)R by using Huygens software (0.67 ± 0.07 [n = 3] and 0.72 ± 0.13 [n = 3], respectively).

To test whether ZIP7 and ZnT7 localizes to the Golgi apparatus, we used a combination of antibodies for either GM130 and ZIP7 or GM130 and ZnT7. Images are shown in Fig. 2*C* and *D*. The merged visual inspections show the presence of the minority of either ZIP7 or ZnT7 to the Golgi. For colocalization, Pearson correlation coefficients for ZIP7 and ZnT7 associated with the Golgi were 0.29 ± 0.02 (n = 3) and 0.51 ± 0.06 (n = 3), respectively.

High-Glucose Treatment Does Not Alter ZIP7 and ZnT7 Intracellular Locations and Calculated Colocalization Values

To test whether hyperglycemia affects the location of ZIP7 and ZnT7 in cells, high-glucose–treated (25 mmol/L for 24 h) cells transfected with DsRed-ER were visualized.

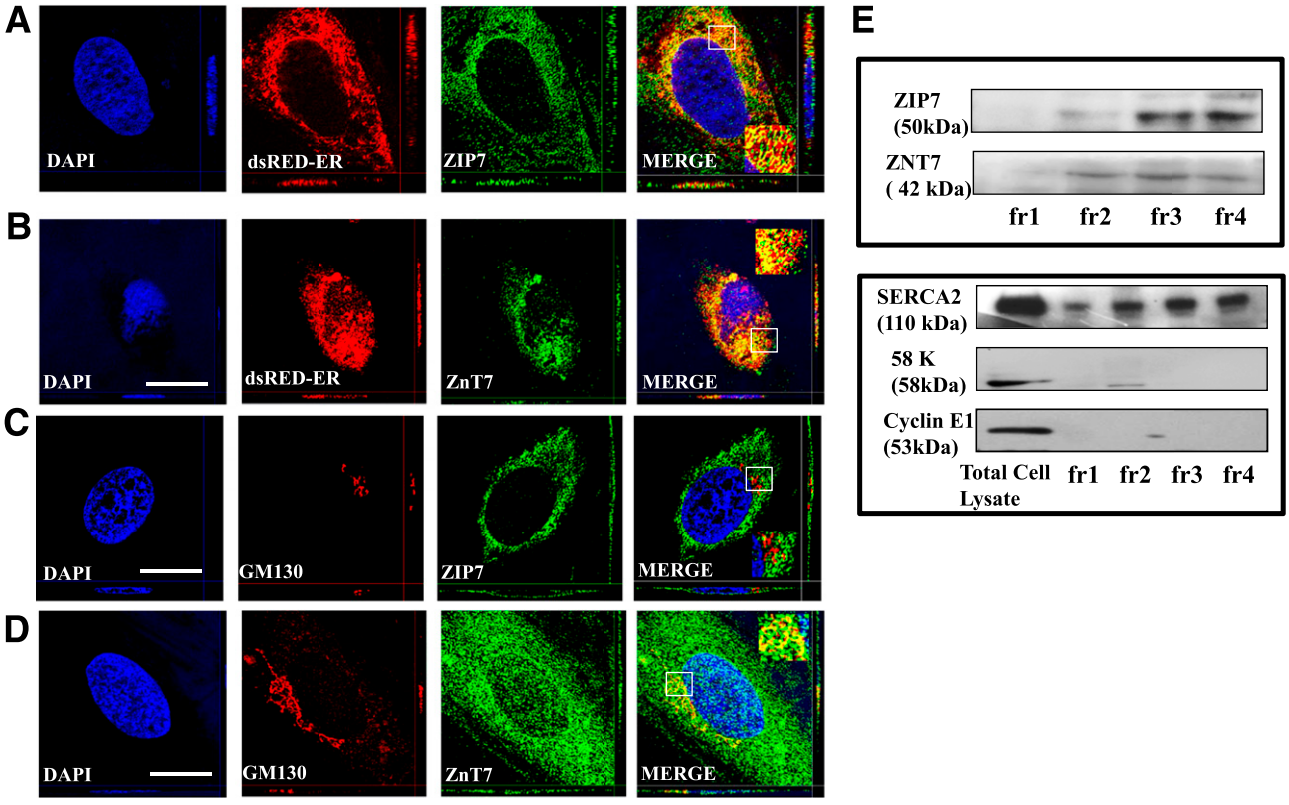


Figure 2—Visualization of ZIP7 and ZnT7 localization to the S(E)Rin H9c2 cells. Localizations of either ZIP7 or ZnT7 to either the S(E)R (*A* and *B*) or the Golgi apparatus (*C* and *D*) were visualized by using confocal micrographs in H9c2 cells. To examine the subcellular localizations of ZIP7 or ZnT7 to S(E)R, H9c2 cells were transfected with DsRed-ER to label ER or incubated with GM130 antibody to label the Golgi apparatus. All cells were fixed and permeabilized (RESEARCH DESIGN AND METHODS). DsRed-ER–transfected cells were incubated with specific ZIP7 or ZnT7 primary antibodies and were followed by secondary antibodies (Alexa Fluor 488 donkey anti-rabbit IgG or Alexa Fluor 488 donkey anti-goat IgG, respectively). To test their possible Golgi localizations (*C* and *D*), the nontransfected cells were incubated with either ZIP7 or ZnT7 primary antibodies and GM130 primary antibody and then followed by secondary antibodies (Alexa Fluor 488 donkey anti-rabbit IgG and Alexa Fluor 568 goat anti-mouse IgG or Alexa Fluor 488 donkey anti-goat IgG and Alexa Fluor 568 rabbit anti-mouse IgG, respectively). The cells were mounted in medium containing DAPI (blue to stain nuclei). Single optical sections (top panels) and representative *z*-plane reconstructions (side and bottom panels) are shown. The insets show a magnified region. Scale bars = 10 μm. For colocalization, Pearson correlation coefficients were calculated for ZIP7 and ZnT7 associated with S(E)R by using Huygens software (*E*). Either ZIP7 or ZnT7 individual localization to the S(E)R was investigated with Western blot analysis in isolated S(E)R fractions (fr1–fr4). Immunoblotting detected either ZIP7 or ZnT7 in all four fractions containing S(E)R membranes. For validation of S(E)R isolation, SERCA2a (sc-8094; Santa Cruz), Golgi 58K Protein (ab27043; Abcam), and cyclin E (sc-481; Santa Cruz) were used as S(E)R, Golgi, and nuclear markers, respectively. The levels of these three markers in total cell lysate are also shown in *E*.

Confocal images are shown in Supplementary Fig. 2*A–D*. For colocalization of ZIP7 and ZnT7 in the S(E)R, Pearson correlation coefficients were calculated as 0.42 ± 0.09 (n = 3) and 0.54 ± 0.08 (n = 3). For colocalization of ZIP7 and ZnT7 in the Golgi apparatus, Pearson correlation coefficients were 0.11 ± 0.02 (n = 3) and 0.70 ± 0.08 (n = 3).

For a comparison of the effects of hyperglycemia on subcellular localizations of ZIP7 and ZnT7, we compared the calculated Pearson correlation coefficients in normal and hyperglycemic cells. Except for ZIP7 localization to the Golgi, localizations of other transporters was unaffected by hyperglycemia (Supplementary Fig. 3*E*).

Validation of ZIP7 and ZnT7 Localizations by Using Western Blotting in Isolated S(E)R

The S(E)R localization of ZIP7 and ZnT7 was further investigated by Western blot in isolated S(E)R fractions (range 1–4) obtained from rat heart. The intensities of protein bands associated with either ZIP7 or ZnT7 showed both a gradually increasing strength from rough to smooth fractions of isolated S(E)R preparation (Fig. 2*E*). These data strongly demonstrate the presence of these two transporters in the smooth part of S(E)R. For further validation of their presence in S(E)R fractions, we assessed SERCA2a (110 kDa) as a positive control and Golgi marker (Golgi 58K Protein) and a nuclear marker cyclin E (53 kDa) as negative controls in the same S(E)R preparations (Fig. 2*E*). The last two markers were clearly observed in total cell lysate as well.

FRET-Based Measurement of Cytosolic and S(E)R Free Zn^{2+} Levels

By using FRET Zn^{2+} probes (10,25), we measured free Zn^{2+} levels in cytosol and S(E)R in H9c2 cells after culture at normal (5.5 mmol/L) or high (25 mmol/L) glucose for 24 h. Representative free Zn^{2+} measurements (RESEARCH DESIGN AND METHODS) are shown in Fig. 3*A* and *B* (for cytosol and S(E)R, respectively). By using quantification from fluorescence intensity (10), Cyt-eCALWY4–infected and

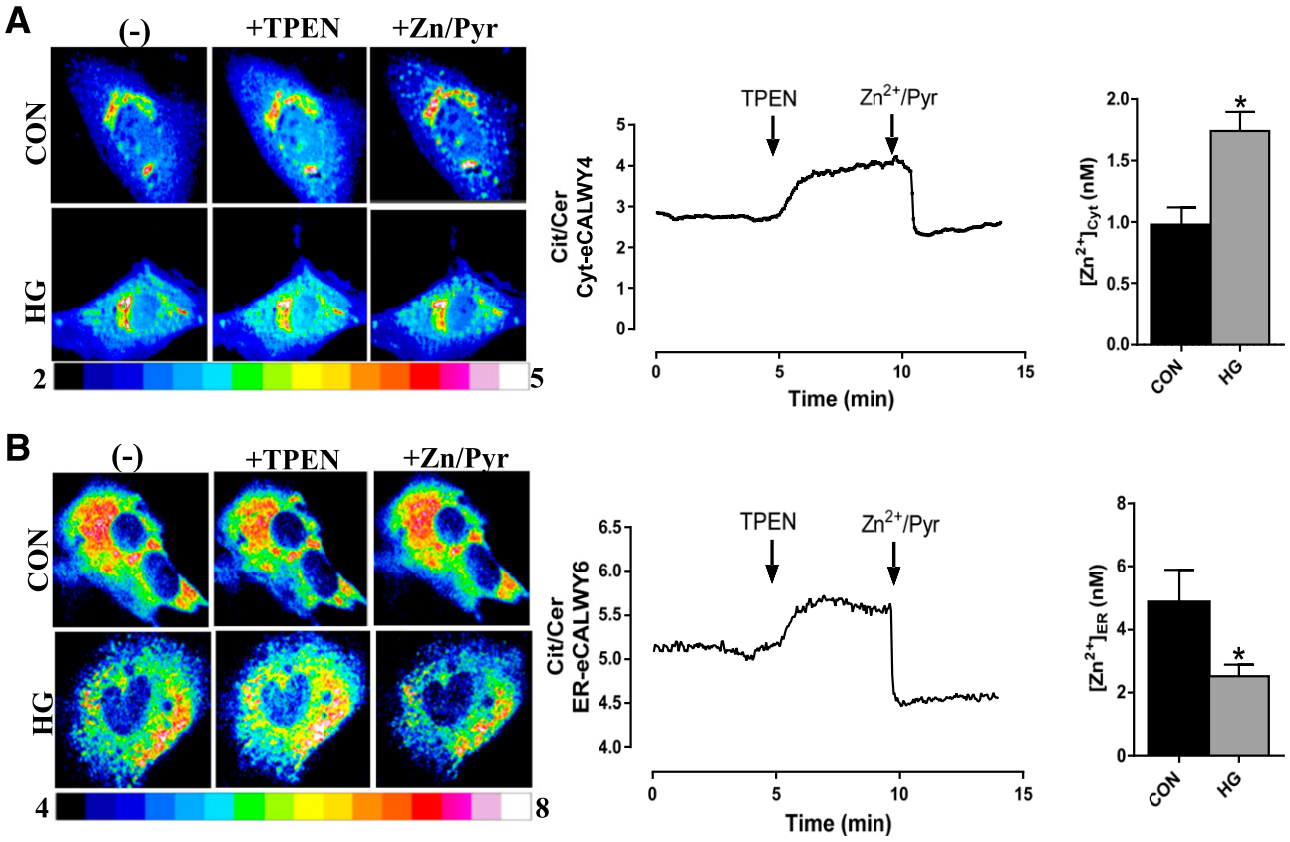


Figure 3—FRET-based measurements of subcellular free Zn^{2+} concentrations in hyperglycemic H9c2 cells by using eCALWY probes. Representative traces (top) and ratiometric images (bottom) are shown for H9c2 cells expressing cytosolic (*A*) or ER-targeted (*B*) sensors. Acquisitions were performed 24 h after transfection or infection and during perfusion with Krebs HEPES-bicarbonate buffer. Steady-state fluorescence intensity ratio (citrine/cerulean [Cit/Cer]) was first measured before the maximum ratio was obtained under perfusion with KHB buffer containing 50 μmol/L TPEN. Finally, the minimum ratio was obtained under perfusion with KHB buffer containing 5 μmol/L Zn^{2+}/Pyr and 100 μmol/L $ZnCl_2$ (Zn^{2+}-saturated condition). Cells were incubated with high glucose (HG) (25 mmol/L for 24 h), and the cytosolic and ER free Zn^{2+} levels are shown for comparison with the controls (CON). The cytosolic free Zn^{2+} levels in Cyt-eCALWY4–infected and HG-incubated H9c2 cells vs. CON are 1.74 ± 0.15 vs. 0.97 ± 0.14 nmol/L (n = 27 vs. 31 cells with eight independent experiments), whereas the S(E)R free Zn^{2+} levels in ER-eCALWY6–infected HG-treated cells vs. CON range from 2.52 ± 0.36 to 4.88 ± 1.00 nmol/L (n = 22 vs. 26 cells with eight independent experiments). Data are mean ± SEM (n >20 cells in every protocol). *P < 0.05 vs. CON.

high-glucose–incubated H9c2 cells showed significantly high cytosolic free Zn^{2+} levels compared with controls (1.74 ± 0.15 vs. 0.97 ± 0.14 nmol/L), whereas S(E)R free Zn^{2+} levels compared with controls ranged from 4.88 ± 1.00 to 2.52 ± 0.36 nmol/L.

Of note, the total cellular free Zn^{2+} level in high-glucose–treated cells was lower than in control cells. Several reasons are possible for these differences. ZnTs located on sarcolemma might be activated by hyperglycemia. Alternatively, high cytosolic Zn^{2+} levels might result Zn^{2+} increases in other organelles, such as mitochondria, through the kinetic activation of uptake pathways (10).

Redistribution of Cellular Free Zn^{2+} in Hyperglycemic Cardiomyocytes Depends on ZIP7 Phosphorylation

Because the demonstration of ZIP7 and ZnT7 localizations to the S(E)R provides further evidence of the role of the S(E)R as an intracellular Zn^{2+} pool in cardiomyocytes (3), with high mRNA and protein levels of ZIP7 and high ZIP7 phosphorylation (rather than ZnT7) under hyperglycemia, we assessed the direct role of S(E)R in the redistribution of cellular free Zn^{2+} in hyperglycemic cardiomyocytes. We first silenced ZIP7 in H9c2 cells. The mRNA levels of ZIP7 and ZnT7 in ZIP7-silenced cells compared with sc-shRNA cells are shown in Fig. 4*A* and *B* (left). The ZIP7 mRNA level was reduced (>60%) compared with controls, whereas the ZnT7 mRNA level was not changed. As expected, ZIP7 immunoreactivity was reduced by >90% in silenced cells with no change in ZnT7 protein levels (Fig. 4*A* and *B*, right).

To test the role of ZIP7 in subcellular Zn^{2+} distribution further, we measured cytosolic and S(E)R free Zn^{2+} levels in nontargeted and ZIP7-targeted shRNA-infected cells by using previously mentioned protocols (RESEARCH DESIGN AND METHODS). As shown in Fig. 4*C* (left), cytosolic free Zn^{2+} was increased more than threefold in hyperglycemic cells compared with control cells (0.92 ± 0.14 vs. 3.28 ± 0.65 nmol/L; n = 36–45 cells). Furthermore, the cytosolic free Zn^{2+} in ZIP7-silenced cells under hyperglycemic conditions was not different from that of ZIP7-silenced cells under physiological conditions (Fig. 4*C*, right). However, the S(E)R free Zn^{2+} in nontargeted shRNA-infected hyperglycemic cells had trended less (36%) (Fig. 4*D*, left). Furthermore, the free Zn^{2+} level in S(E)R in ZIP7-silenced cells under hyperglycemic conditions was not different from that of ZIP7-silenced cells under physiological conditions

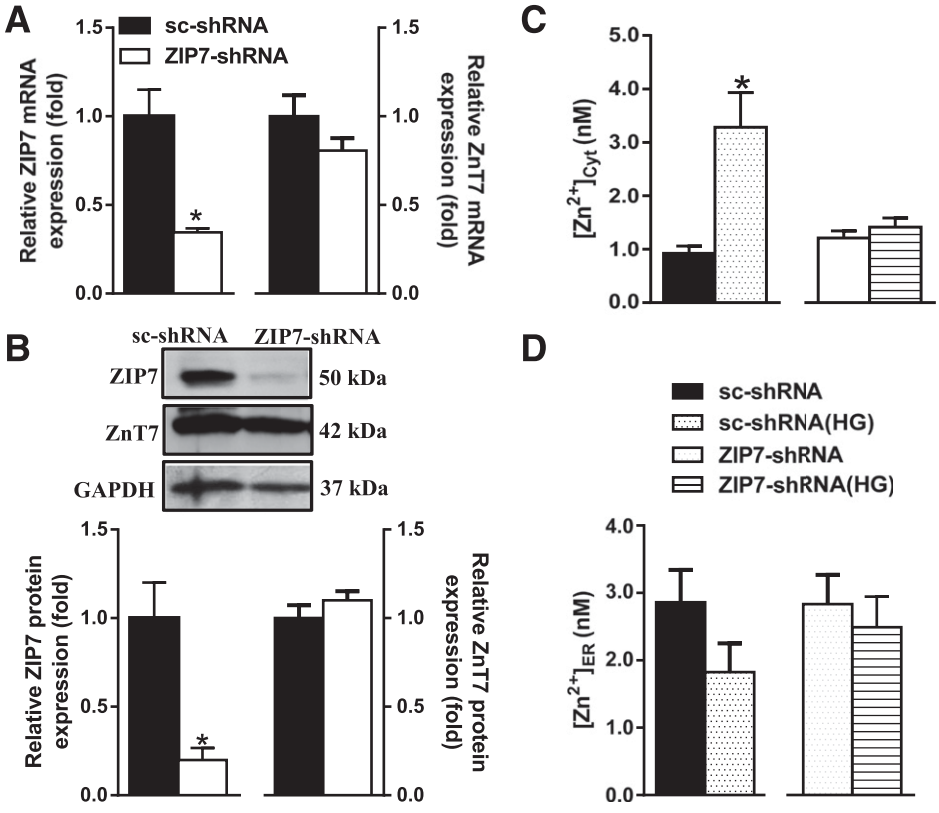


Figure 4—Confirmation of ZIP7 silencing and FRET-based measurements of cytosolic or S(E)R free Zn^{2+} concentrations in H9c2 cells cultured under hyper- or normoglycemic conditions. The ZIP7 silencing was confirmed by measuring ZIP7 and ZnT7 mRNA (*A*) and protein (*B*) levels with respect to sc-shRNA–infected cells. ZIP7 silencing does not affect ZnT7 mRNA (*A*) or protein (*B*) levels. The cytosolic (*C*) and S(E)R (*D*) free Zn^{2+} levels measured in ZIP7 silenced H9c2 cells under hyperglycemic conditions as expressed by eCALWY sensors (FRET measurements were carried out as for Fig. 3) compared with those in sc-shRNA–treated cells. Data are mean ± SEM (n = 8–36 cells for each protocol from three independent experiments). *P < 0.05 vs. sc-shRNA. HG, high glucose.

(Fig. 4*D*, right). These results are consistent with an important role for S(E)R-localized ZIP7 in the redistribution of subcellular Zn^{2+} in cardiomyocytes under hyperglycemia.

Alterations in ZIP7 and ZnT7 Expressions Cause ER Stress Through Loss of S(E)R Free Zn^{2+} Under Hyperglycemia

Previously, marked ER stress and increased intracellular free Zn^{2+} in isolated left-ventricular cardiomyocytes from DM rats have been shown (4,29,30) and demonstrated an ER Zn^{2+} deficiency–associated disruption in its function and induction of ER stress in eukaryotes (14). Therefore, we hypothesized that similar changes in cardiomyocytes would lead to ER stress under hyperglycemia. To test this hypothesis, we first measured ER stress chaperone levels of GRP78 and CALR in high-glucose–incubated cells (25 mmol/L for 24 h) compared with those of control cells. The GRP78 and CALR levels were increased significantly in hyperglycemic cells similar to those DM rat heart tissue (32) (Fig. 5*A*). We also examined GRP78 induction in response to a direct ER stress activator tunicamycin (TUN) (10 μmol/L for 18 h) and again showed increased GRP78 expression levels (Fig. 5*B*). To demonstrate a hypothesis related to hyperglycemia-associated changes in protein expression levels of these transporters can underlie the induction of ER stress in cardiomyocytes, we used direct ER stress–induced cardiomyocytes with TUN incubation and measured ZIP7 and ZnT7 expression levels, which were not significantly different from those of controls (Fig. 5*C* and *D*).

Hyperglycemia-Associated ZIP7 Phosphorylation

Because we observed a markedly higher ZIP7 phosphorylation level in DM rat cardiomyocytes (Fig. 1*E*) and high-glucose–incubated cells (Fig. 1*F*) versus their respective controls, we aimed to clarify whether these changes arose as a direct consequence of ER stress. To address this prediction, we treated cells with 10 μmol/L TUN for 24 h to induce ER stress directly and then measured pZIP7 levels. No significant differences were found between treated and untreated cells, implying no direct ER stress effect

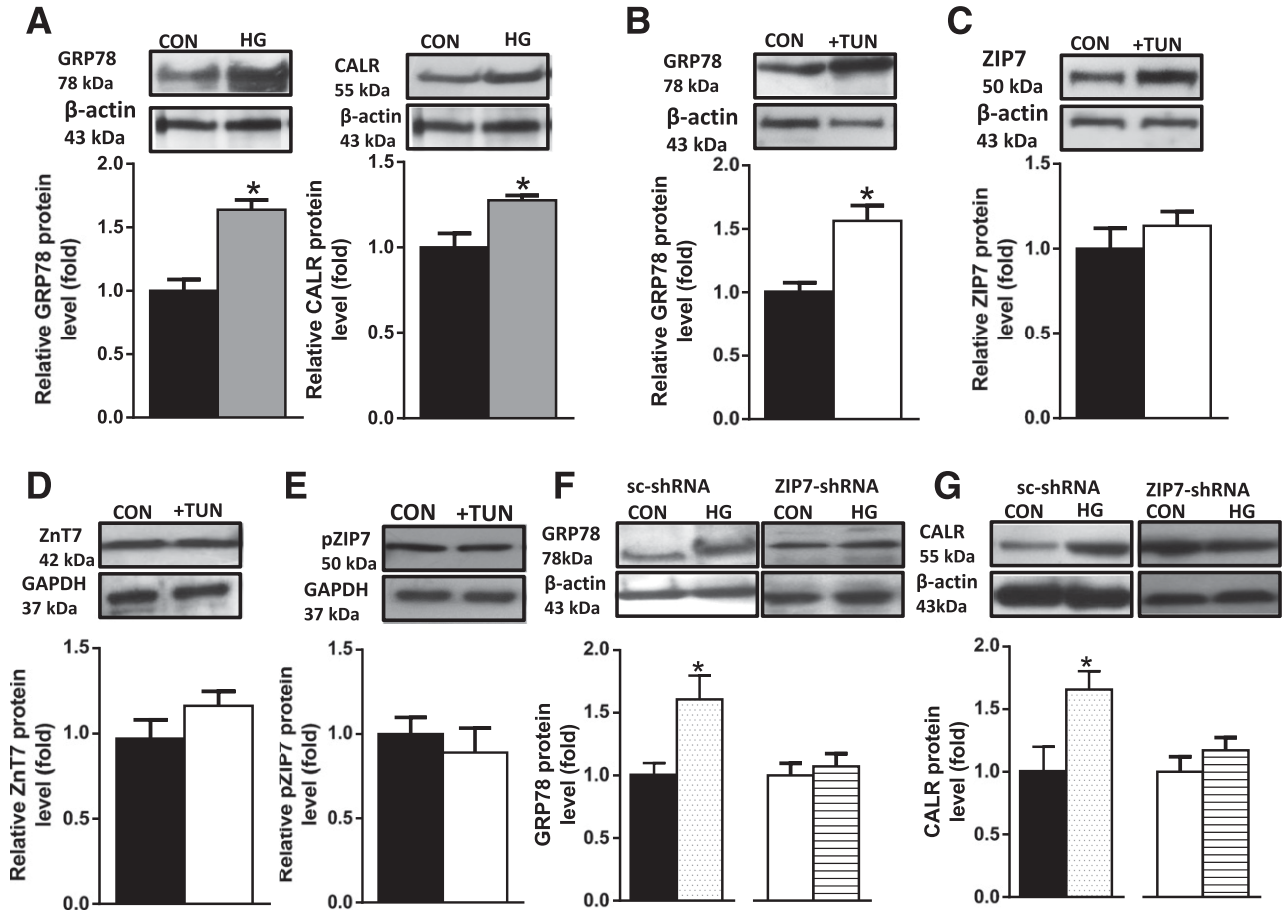


Figure 5—The in vitro induction and confirmation of ER stress in H9c2 cells. *A*: To test whether hyperglycemia induces changes in the protein levels of ZIP7 and ZnT7 and, in turn, further underlies the induction of ER stress in H9c2 cells, two molecular chaperones, GRP78 and CALR were measured by Western blotting, in control or high-glucose (HG) (25 mmol/L for 24 h)–incubated H9c2 cells. *B*: GRP78 was measured under direct ER stress induction with TUN. *C* and *D*: Protein levels of ZIP7 and ZnT7 were measured after ER stress induction with TUN. *E*: pZIP7 protein levels were measured in H9c2 cells incubated with TUN with respect to GAPDH as the reference protein. *F* and *G*: GRP78 and CALR protein levels measured in ZIP7-silenced cells. Data are mean ± SEM and were obtained after duplicate assays of each sample from each group for each type of measurement. *$P < 0.05$ vs. controls (CON) or sc-shRNA (CON).

on ZIP7 phosphorylation (Fig. 5*E*). For further support associated with ZIP7-induced ER stress, we monitored expression levels of GRP78 and CALR in ZIP7-silenced cells under hyperglycemic conditions and found no difference from those of respective control conditions (Fig. 5*F* and *G*).

For further support of the association between activation of ZIP7-related increased cytosolic Zn^{2+} under hyperglycemia and ER stress induction, we increased cytosolic free Zn^{2+} through Zn^{2+}/Pyr (100 nmol/L for 24 h). We then measured markedly increased GRP78 and CALR levels while these levels could be reversed to control levels with the ER stress inhibitor tauroursodeoxycholic acid (50 μmol/L for 24 h) (Supplementary Fig. 5*A* and *B*). The above results thus provide further support for the view that hyperglycemia-associated changes in pZIP7 and ZIP7 levels underlie an induction of ER stress.

CK2α Activation in Diabetic Heart Is Associated With Both Hyperglycemia- and Hyperglycemia-Induced Cytosolic Free Zn^{2+} Increase

CK2α is an unusual protein kinase, being constitutively active, and undergoes autophosphorylation (33). Both CK2α activity and expression are increased with low Zn^{2+} levels in a concentration-dependent manner (34). Because CK2α activation has been shown previously to prompt cytosolic Zn^{2+} signaling (18) and high-glucose (0–25 mmol/L) treatment (for 4 h) of cells induces significant CK2α activity in a concentration-dependent manner (35), we first examined CK2α expression in isolated cardiomyocytes from DM rat heart and then in Zn^{2+}/Pyr-incubated (1 μmol/L for 20 min) rat cardiomyocytes compared with those of controls. Both CK2α expressions were significantly higher than in their respective controls (Fig. 6*A*). Furthermore, we repeated similar measurements in H9c2 cells maintained at high glucose (25 mmol/L for 24 h) or Zn^{2+}/Pyr (1 μmol/L for 20 min). High-glucose incubation for 24 h induced a significant increase in CK2α expression (twofold), whereas an eightfold increase was observed in CK2α expression in the Zn^{2+}/Pyr-incubated cells for 20 min (Fig. 6*B*). These data demonstrate that CK2α expression increases in response to hyperglycemia or elevated cytosolic free Zn^{2+} and might contribute in a feed-forward cycle to further Zn^{2+} release into cytoplasm.

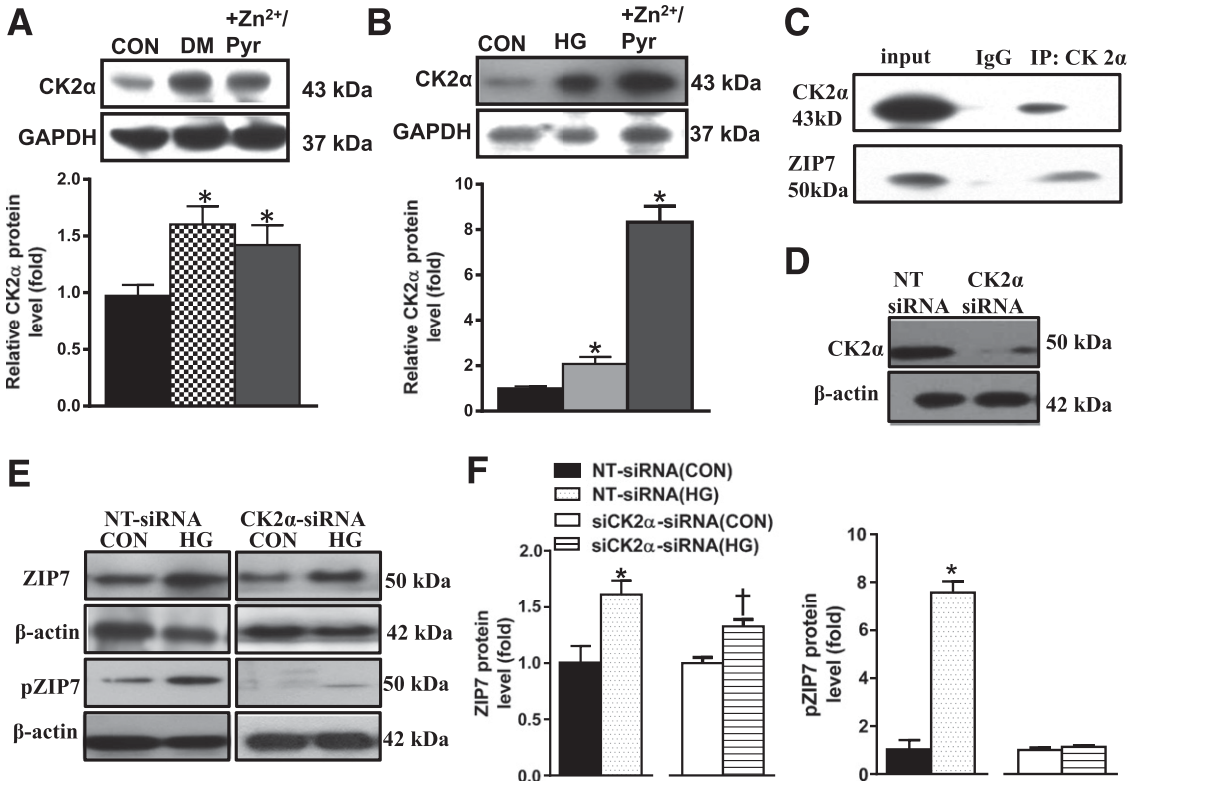


Figure 6—Activated CK2α in DM rat heart cells and high-glucose (HG)– or Zn^{2+}/Pyr-incubated H9c2 cells and demonstration of colocalization of CK2α and ZIP7. *A*: The protein level of protein kinase CK2α measured at 43 kDa in cardiomyocytes from normal control (CON) and DM rats and isolated cardiomyocytes incubated with Zn^{2+}/Pyr (1 μmol/L for 20 min). *B*: H9c2 cells incubated either with HG (25 mmol/L for 24 h) or Zn^{2+}/Pyr (1 μmol/L for 20 min). *C*: To determine whether ZIP7 phosphorylation is associated with high CK2α expression or vice versa in hyperglycemia-exposed cells, coimmunoprecipitation experiments were performed by using anti-ZIP7 antibody, and the precipitates were probed for CK2α in H9c2 cells. *D*: Confirmation of CK2α silencing by using Western blotting. *E* and *F*: The protein levels of pZIP7 and ZIP7 in both nontargeted (NT)-siRNA– or CK2α-siRNA–transfected cells with either hyperglycemic (HG) or normoglycemic (CON) conditions were measured and compared between groups. Data are mean ± SEM and were obtained with double assays in each sample from each group for each type of measurement. **P* < 0.05 vs. CON or NT-siRNA (CON); †*P* < 0.05 vs. CK2α-siRNA (CON). IP, immunoprecipitation.

On the basis of data shown in Fig. 1*F*, the importance of time dependency of hyperglycemia-associated elevated cytosolic free Zn^{2+} effect on pZIP7 expression is emphasized.

CK2α Contributes to Activation of ZIP7 Through ZIP7 Phosphorylation in Hyperglycemia

Because of the association among CK2α activation/expression, ZIP7 phosphorylation, and Zn^{2+} influx into the cytoplasm from the ER previously reported in tamoxifen-resistant breast cancer cells (18), we performed coimmunoprecipitation measurements in H9c2 cells (Fig. 6*C*). These data reveal an association between CK2α activation (at most as a result of hyperglycemia) and increased cytosolic free Zn^{2+}-dependent phosphorylation and activation of ZIP7 in response to hyperglycemia.

To test whether ZIP7 may be phosphorylated by other kinases, which also are activated by increased intracellular Zn^{2+} in cardiomyocytes (4,30,36), we performed further coimmunoprecipitation experiments by using various antibodies against them. We did not observe coimmunoprecipitation between ZIP7 and any of the other kinases.

To validate the essentiality of CK2α activation for ZIP7 phosphorylation, we silenced CK2α in normal and high-glucose–treated (25 mmol/L for 24 h) H9c2 cells and then measured pZIP7 and ZIP7 expression levels. CK2α protein level is markedly reduced in CK2α-silenced cells (Fig. 6*D*), whereas the mRNA levels of CK2α1 and CK2α2 are decreased (Supplementary Fig. 6). In addition, no ZIP7 phosphorylation was observed in CK2α-silenced cells under control or hyperglycemic conditions, whereas a sevenfold increased pZIP7 in nontarget siRNA–transfected hyperglycemic cells was observed (Fig. 6*E* and *F*). The ratio of pZIP7/ZIP7 is fivefold higher in hyperglycemia than in normoglycemia in nontargeted siRNA cells. However, silencing of CK2α has not changed this ratio under control and hyperglycemic conditions (Supplementary Fig. 7), suggesting the importance of increased ZIP7 phosphorylation in response to hyperglycemia.

DISCUSSION

Our overall aim was to examine roles of Zn^{2+} carriers ZIP7 and ZnT7 in cardiomyocytes under physiological conditions and as potential mediators of ER stress in hyperglycemia- and hyperglycemia-induced cardiac dysfunction. The results suggest that these Zn^{2+} carriers are likely to carry Zn^{2+} in opposite directions across the S(E)R membrane. Furthermore, we show that increased ZIP7 levels together with increased ZIP7 phosphorylation were likely to drive changes in S(E)R lumen and cytosol with deleterious consequences for cell function in both cases. Although not assessed directly, lowered ZnT7 expression under hyperglycemia, particularly under chronic conditions, is likely to further exacerbate these changes and contribute to deleterious consequences of Zn^{2+} redistribution between compartments. Of note, these transporters localize into the S(E)R membrane and may thus operate as functional proteins catalyzing Zn^{2+} release and uptake from the S(E)R.

To the best of our knowledge, this study is the first to assess both localization and functional roles of ZIP7 and ZnT7 as working in opposing directions in mammalian heart and, most importantly, their contributions to diabetic cardiac dysfunction through ER stress. In addition, we demonstrate markedly increased CK2α expression under hyperglycemia (at most through hyperglycemia activation of CK2α [35]) and provide evidence that this can lead to phosphorylation of the channel on residues previously implicated in control of Zn^{2+} release (18). In particular, our experiments that used CK2α-silenced cells provide further support for this view. Thus, a combination of transcriptional and posttranscriptional mechanisms may contribute to ZIP7 activation in hyperglycemia. Increases in both expression and phosphorylation of ZIP7 under hyperglycemia are time dependent, and the ZIP7 phosphorylation increase is significantly higher than that in chronic hyperglycemia, indicating a role of ZIP7 activation in cardiomyocytes in diabetes.

The data provide further evidence of a role for the S(E)R as an intracellular Zn^{2+} pool, contributing to Zn^{2+} regulation in cardiomyocytes, in a process controlled by ZIP7 and ZnT7. In this regard, S(E)R Zn^{2+} deficiency has been shown to induce unfolded protein response (14) and that Zn^{2+} homeostasis is involved through a putative ZnT localized to the S(E)R (37). Moreover, high glucose has been demonstrated to induce a stable increase in cytosolic Zn^{2+} in pancreatic β-cells and to lead to profound alterations in expression of genes important for Zn^{2+} homeostasis, such as a ZIP7 increase (25). Therefore, the current data are noteworthy when considering ZIP7 and ZnT7 roles located into the S(E)R and responsible for ER stress in part as a result of depressed S(E)R free Zn^{2+}.

Cytosolic Zn^{2+} increase in cardiomyocytes can induce marked high phosphorylation in many kinases and oxidation of proteins responsible for heart function (3,4,30,38), which is consistent with previous studies on the role of ZIP7 in control of Zn^{2+} release from the S(E)R in cancer cells (17,18). In support of these earlier findings, we show that CK2α is activated in hyperglycemic cardiomyocytes and directly activated with increased cytosolic Zn^{2+} levels. More importantly, these observations support our present hypothesis. Indeed, CK2α plays a key role in the regulation of prosurvival as well as proapoptotic ER stress signaling by directly modulating the activities of ER stress–signaling actors by phosphorylation, regulating expression of the key factors of signaling pathways or binding to regulator proteins (39).

Little is known about cytosolic Zn^{2+}, ZnTs, and cardiovascular complications. Early studies demonstrated that ZIP7 is involved in Zn^{2+} homeostasis of the Golgi apparatus (15). Although ZIP7 and ZnT7 have been shown to be weakly expressed in mammalian heart (22,23), we observed marked ZIP7 and ZnT7 protein levels in DM rat heart, although others have demonstrated a correlation among increased reactive oxygen species, ER stress, and CK2α activation (36,40) through cellular control of Zn^{2+} distribution with CK2α-mediated ZIP7 phosphorylation (18). Therefore, the current data represent a first investigation into the role of CK2α-mediated ZIP7 phosphorylation and

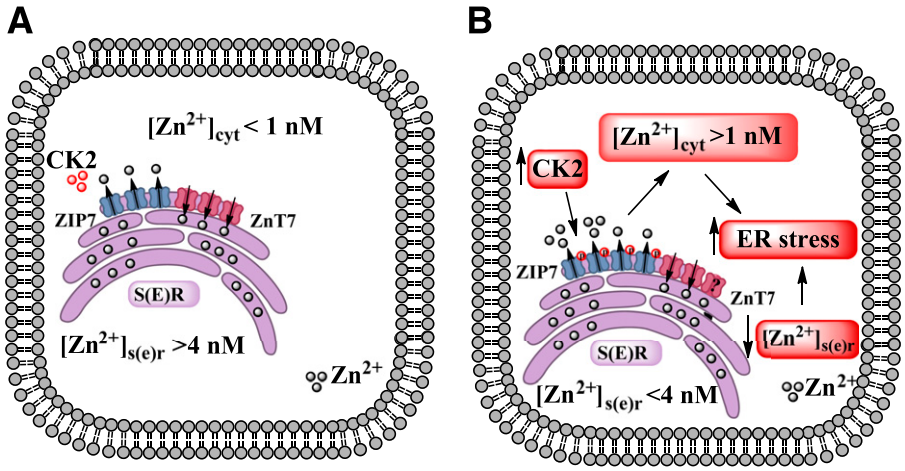


Figure 7—Schematic illustration of the regulation of Zn^{2+} homeostasis in cardiomyocytes under physiological and hyperglycemic conditions. *A*: Regulation of cellular distribution of free Zn^{2+} through a ZIP7/ZnT7 system localized to the S(E)R in resting cardiomyocytes. *B*: When cardiomyocytes are exposed to high glucose, CK2α becomes activated, inducing the phosphorylation of ZIP7 (18) and Zn^{2+} influx into cytosol from the S(E)R. Downregulation of ZnT7 may further contribute to this process. In addition, high glucose can stimulate an increase of cytosolic free Zn^{2+} through mobilization of Zn^{2+} from metalloproteins (5,30,44,45), which in turn induces phosphorylation of several endogenous proteins (30,44–46). The changes in both cytosolic and S(E)R free Zn^{2+} levels under hyperglycemic conditions are shown compared with controls. Consequently, cytosolic free Zn^{2+} increase through one or two ways underlies induction of ER stress through overexpression of ER stress chaperones in cardiomyocytes under high-glucose conditions.

Zn^{2+} homeostasis in cardiomyocytes under hyperglycemia and further propose a protective role for ZnT7 against oxidative stress or high susceptibility to diet-induced glucose intolerance/insulin resistance (24,41).

Hyperglycemia induces cardiac dysfunction as a result of increased oxidative and ER stress (42,43). The current data reinforce the hypothesis of an S(E)R role as an important Zn^{2+} pool in cardiomyocytes with ZIP7 and ZnT7 localization into the S(E)R and make an important contribution to Zn^{2+} homeostasis. Nonetheless, we also recognize a possible contribution of other ZnTs that contribute to ER stress in cardiomyocytes under hyperglycemia. The data, therefore, provide important information related to Zn^{2+} homeostasis through ZIP7 and ZnT7 functioning as opposing ZnTs localized to the S(E)R in cardiomyocytes. Perturbed expression of either or both transporters may lead to altered Zn^{2+} distribution across the S(E)R and lead to persistent ER stress.

Zn^{2+} homeostasis in cardiomyocytes under physiological and hyperglycemic conditions is summarized in Fig. 7. Regulation of subcellular free Zn^{2+} distribution is proposed to occur through the ZIP7/ZnT7 system localized to the S(E)R. When cardiomyocytes are exposed to high glucose, CK2α becomes activated, inducing a Zn^{2+} influx into cytosol from S(E)R through ZIP7 phosphorylation (18), although a downregulated ZnT7 may further contribute to this process. High glucose also stimulates a cytosolic free Zn^{2+} increase through mobilization of Zn^{2+} from metalloproteins (5,30,44,45), which in turn induce phosphorylation of several proteins (30,45,46). Of note, the latter might further stimulate ZIP7 activity and may lead to accelerated Zn^{2+}-influx into cytosol from the S(E)R. Consequently, cytosolic free Zn^{2+} increases driven by multiple mechanisms lead to ER stress through and the overexpression of ER stress chaperones in cardiomyocytes during hyperglycemia. The current data provide novel insights into regulation of cellular Zn^{2+} and its role in hyperglycemia/diabetes-associated cardiac dysfunction. In addition, the findings may provide new targets, such as cellular Zn^{2+} regulation through mediation of ZnTs, and suggest that modulation of CK2α provides a novel means to correct diabetes-induced cardiac dysfunction.

Acknowledgments. The authors thank Yusuf Olgar (Department of Biophysics, Faculty of Medicine, Ankara University, Ankara, Turkey) for contributions to some of the Western blot analyses. The authors also thank Dr. Angeles Mondragon (Imperial College London) for assistance with plasmid amplification and virus production and Steve Rothery (Imperial College London) for assistance with imaging experiments.

Funding. E.T. acknowledges receipt of a European Cooperation in Science and Technology COST action STSM TD1304 grant and thanks the European Foundation for the Study of Diabetes for an Albert Renold Travel Fellowship. G.A.R. thanks the Medical Research Council (U.K.) for programme grant MR/J0003042/1, the Biotechnology and Biological Sciences Research Council (U.K.) for project grant BB/J015873/1, and the Royal Society for a Wolfson Research Merit Award and the Wellcome Trust for a Senior Investigator Award (WT098424AIA). B.T. thanks the Scientific and Technological Research Council of Turkey for grant SBAG-113S466 and COST action TD1304. K.M.T. thanks the Wellcome Trust University Research Award (grant number 091991/Z/10/Z).

Duality of Interest. No potential conflicts relevant to this article were reported.

Authors Contributions. E.T. performed the electrophysiological and imaging experiments, contributed to all biochemical and molecular biology experiments, and analyzed all experimental data and confocal images. V.C.B. and A.D. performed all biochemical and molecular experiments. G.R.J.C. contributed to the knockdown experiments. K.M.T. provided the antibody for ZIP7 and contributed to the discussion. G.A.R. supported the experimental data in his

laboratory and reviewed and edited the manuscript. B.T. designed the study, wrote the manuscript, researched data, and provided funding for the study. B.T. is the guarantor of this work and, as such, had full access to all the data in the study and takes responsibility for the integrity of the data and the accuracy of the data analysis.

Prior Presentation. Parts of this study were presented in abstract form at the Biophysical Society 60th Annual Meeting, Los Angeles, CA, 27 February–2 March 2016.

References

1. Choi KM, Zhong Y, Hoit BD, et al. Defective intracellular Ca(2+) signaling contributes to cardiomyopathy in type 1 diabetic rats. Am J Physiol Heart Circ Physiol 2002;283:H1398–H1408
2. Yaras N, Ugur M, Ozdemir S, et al. Effects of diabetes on ryanodine receptor Ca release channel (RyR2) and Ca2+ homeostasis in rat heart. Diabetes 2005;54: 3082–3088
3. Tuncay E, Bilginoglu A, Sozmen NN, et al. Intracellular free zinc during cardiac excitation-contraction cycle: calcium and redox dependencies. Cardiovasc Res 2011;89:634–642
4. Tuncay E, Okatan EN, Vassort G, Turan B. β-blocker timolol prevents arrhythmogenic Ca^{2+} release and normalizes Ca^{2+} and Zn^{2+} dyshomeostasis in hyperglycemic rat heart. PLoS One 2013;8:e71014
5. Turan B, Fliss H, Désilets M. Oxidants increase intracellular free Zn2+ concentration in rabbit ventricular myocytes. Am J Physiol 1997;272:H2095–H2106
6. Tuncay E, Turan B. Intracellular Zn(2+) increase in cardiomyocytes induces both electrical and mechanical dysfunction in heart via endogenous generation of reactive nitrogen species. Biol Trace Elem Res 2016;169:294–302
7. Atar D, Backx PH, Appel MM, Gao WD, Marban E. Excitation-transcription coupling mediated by zinc influx through voltage-dependent calcium channels. J Biol Chem 1995;270:2473–2477
8. Hirano T, Murakami M, Fukada T, Nishida K, Yamasaki S, Suzuki T. Roles of zinc and zinc signaling in immunity: zinc as an intracellular signaling molecule. Adv Immunol 2008;97:149–176
9. Woodier J, Rainbow RD, Stewart AJ, Pitt SJ. Intracellular zinc modulates cardiac ryanodine receptor-mediated calcium release. J Biol Chem 2015;290: 17599–17610
10. Chabosseau P, Tuncay E, Meur G, et al. Mitochondrial and ER-targeted eCALWY probes reveal high levels of free Zn2+. ACS Chem Biol 2014;9:2111–2120
11. Kambe T, Tsuji T, Hashimoto A, Itsumura N. The physiological, biochemical, and molecular roles of zinc transporters in zinc homeostasis and metabolism. Physiol Rev 2015;95:749–784
12. Chabosseau P, Rutter GA. Zinc and diabetes. Arch Biochem Biophys 2016; 611:79–85
13. Kimura T, Kambe T. The functions of metallothionein and ZIP and ZnT transporters: an overview and perspective. Int J Mol Sci 2016;17:336
14. Ellis CD, Wang F, MacDiarmid CW, Clark S, Lyons T, Eide DJ. Zinc and the Msc2 zinc transporter protein are required for endoplasmic reticulum function. J Cell Biol 2004;166:325–335
15. Huang L, Kirschke CP, Zhang Y, Yu YY. The ZIP7 gene (Slc39a7) encodes a zinc transporter involved in zinc homeostasis of the Golgi apparatus. J Biol Chem 2005;280:15456–15463
16. Hogstrand C, Kille P, Nicholson RI, Taylor KM. Zinc transporters and cancer: a potential role for ZIP7 as a hub for tyrosine kinase activation. Trends Mol Med 2009;15:101–111
17. Taylor KM, Vichova P, Jordan N, Hiscox S, Hendley R, Nicholson RI. ZIP7-mediated intracellular zinc transport contributes to aberrant growth factor signaling in antihormone-resistant breast cancer cells. Endocrinology 2008;149: 4912–4920
18. Taylor KM, Hiscox S, Nicholson RI, Hogstrand C, Kille P. Protein kinase CK2 triggers cytosolic zinc signaling pathways by phosphorylation of zinc channel ZIP7. Sci Signal 2012;5:ra11
19. Liu Y, Batchuluun B, Ho L, et al. Characterization of zinc influx transporters (ZIPs) in pancreatic β cells: roles in regulating cytosolic zinc homeostasis and insulin secretion. J Biol Chem 2015;290:18757–18769
20. Grubman A, Lidgerwood GE, Duncan C, et al. Deregulation of subcellular biometal homeostasis through loss of the metal transporter, Zip7, in a childhood neurodegenerative disorder. Acta Neuropathol Commun 2014;2:25
21. Groth C, Sasamura T, Khanna MR, Whitley M, Fortini ME. Protein trafficking abnormalities in *Drosophila* tissues with impaired activity of the ZIP7 zinc transporter Catsup. Development 2013;140:3018–3027
22. Kirschke CP, Huang L. ZnT7, a novel mammalian zinc transporter, accumulates zinc in the Golgi apparatus. J Biol Chem 2003;278:4096–4102
23. Yang J, Zhang Y, Cui X, et al. Gene profile identifies zinc transporters differentially expressed in normal human organs and human pancreatic cancer. Curr Mol Med 2013;13:401–409
24. Huang L, Kirschke CP, Lay YA, Levy LB, Lamirande DE, Zhang PH. Znt7-null mice are more susceptible to diet-induced glucose intolerance and insulin resistance. J Biol Chem 2012;287:33883–33896
25. Bellomo EA, Meur G, Rutter GA. Glucose regulates free cytosolic Zn^{2+} concentration, Slc39 (ZiP), and metallothionein gene expression in primary pancreatic islet β-cells. J Biol Chem 2011;286:25778–25789
26. Rutter GA, Chabosseau P, Bellomo EA, et al. Intracellular zinc in insulin secretion and action: a determinant of diabetes risk? Proc Nutr Soc 2016;75:61–72
27. Li F, Luo J, Wu Z, et al. Hydrogen sulfide exhibits cardioprotective effects by decreasing endoplasmic reticulum stress in a diabetic cardiomyopathy rat model. Mol Med Rep 2016;14:865–873
28. Yang L, Zhao D, Ren J, Yang J. Endoplasmic reticulum stress and protein quality control in diabetic cardiomyopathy. Biochim Biophys Acta 2015;1852: 209–218
29. Cicek FA, Ozgur EO, Ozgur E, Ugur M. The interplay between plasma membrane and endoplasmic reticulum Ca(2+)ATPases in agonist-induced temporal Ca(2+) dynamics. J Bioenerg Biomembr 2014;46:503–510
30. Tuncay E, Okatan EN, Toy A, Turan B. Enhancement of cellular antioxidant-defence preserves diastolic dysfunction via regulation of both diastolic Zn2+ and Ca2+ and prevention of RyR2-leak in hyperglycemic cardiomyocytes. Oxid Med Cell Longev 2014;2014:290381
31. Harding HP, Ron D. Endoplasmic reticulum stress and the development of diabetes: a review. Diabetes 2002;51(Suppl. 3):S455–S461
32. Cicek FA, Toy A, Tuncay E, Can B, Turan B. Beta-blocker timolol alleviates hyperglycemia-induced cardiac damage via inhibition of endoplasmic reticulum stress. J Bioenerg Biomembr 2014;46:377–387
33. Chester N, Marshak DR. Dimethyl sulfoxide-mediated primer Tm reduction: a method for analyzing the role of renaturation temperature in the polymerase chain reaction. Anal Biochem 1993;209:284–290
34. Gatica M, Hinrichs MV, Jedlicki A, Allende CC, Allende JE. Effect of metal ions on the activity of casein kinase II from *Xenopus laevis*. FEBS Lett 1993;315: 173–177
35. Welker S, Götz C, Servas C, Laschke MW, Menger MD, Montenarh M. Glucose regulates protein kinase CK2 in pancreatic β-cells and its interaction with PDX-1. Int J Biochem Cell Biol 2013;45:2786–2795
36. Yaras N, Tuncay E, Purali N, Sahinoglu B, Vassort G, Turan B. Sex-related effects on diabetes-induced alterations in calcium release in the rat heart. Am J Physiol Heart Circ Physiol 2007;293:H3584–H3592
37. Wang M, Xu Q, Yu J, Yuan M. The putative Arabidopsis zinc transporter ZTP29 is involved in the response to salt stress. Plant Mol Biol 2010;73:467–479
38. Xie H, Zhu PH. Biphasic modulation of ryanodine receptors by sulfhydryl oxidation in rat ventricular myocytes. Biophys J 2006;91:2882–2891
39. Götz C, Müller A, Montenarh M, Zimmermann R, Dudek J. The ER-membrane-resident Hsp40 ERj1 is a novel substrate for protein kinase CK2. Biochem Biophys Res Commun 2009;388:637–642
40. Intemann J, Saidu NE, Schwind L, Montenarh M. ER stress signaling in ARPE-19 cells after inhibition of protein kinase CK2 by CX-4945. Cell Signal 2014;26:1567–1575

41. Liang D, Xiang L, Yang M, et al. ZnT7 can protect MC3T3-E1 cells from oxidative stress-induced apoptosis via PI3K/Akt and MAPK/ERK signaling pathways. Cell Signal 2013;25:1126–1135
42. Bhandary B, Marahatta A, Kim HR, Chae HJ. An involvement of oxidative stress in endoplasmic reticulum stress and its associated diseases. Int J Mol Sci 2012;14:434–456
43. Lakshmanan AP, Harima M, Suzuki K, et al. The hyperglycemia stimulated myocardial endoplasmic reticulum (ER) stress contributes to diabetic cardiomyopathy in the transgenic non-obese type 2 diabetic rats: a differential role of unfolded protein response (UPR) signaling proteins. Int J Biochem Cell Biol 2013; 45:438–447
44. Hao Q, Maret W. Aldehydes release zinc from proteins. A pathway from oxidative stress/lipid peroxidation to cellular functions of zinc. FEBS J 2006;273: 4300–4310
45. Fliss H, Ménard M. Oxidant-induced mobilization of zinc from metallothionein. Arch Biochem Biophys 1992;293:195–199
46. Vassort G, Turan B. Protective role of antioxidants in diabetes-induced cardiac dysfunction. Cardiovasc Toxicol 2010;10:73–86